Letter

ADVANCED PHOTONICS

Topological transformation and free-space transport of photonic hopfions

Yijie Shen,[a,*] Bingshi Yu,[b] Haijun Wu,[b] Chunyu Li,[b] Zhihan Zhu,[b,*] and Anatoly V. Zayats[c,*]
[a]University of Southampton, Optoelectronics Research Centre and Centre for Photonic Metamaterials, Southampton, United Kingdom
[b]Harbin University of Science and Technology, Wang Da-Heng Center, Heilongjiang Key Laboratory of Quantum Control, Harbin, China
[c]King's College London, London Centre for Nanotechnology, Department of Physics, London, United Kingdom

Abstract. Structured light fields embody strong spatial variations of polarization, phase, and amplitude. Understanding, characterization, and exploitation of such fields can be achieved through their topological properties. Three-dimensional (3D) topological solitons, such as hopfions, are 3D localized continuous field configurations with nontrivial particle-like structures that exhibit a host of important topologically protected properties. Here, we propose and demonstrate photonic counterparts of hopfions with exact characteristics of Hopf fibration, Hopf index, and Hopf mapping from real-space vector beams to homotopic hyperspheres representing polarization states. We experimentally generate photonic hopfions with on-demand high-order Hopf indices and independently controlled topological textures, including Néel-, Bloch-, and antiskyrmionic types. We also demonstrate a robust free-space transport of photonic hopfions, thus showing the potential of hopfions for developing optical topological informatics and communications.

Keywords: topology; skyrmions; hopfions; structured light; spin-orbital interaction.

Received Nov. 18, 2022; revised manuscript received Dec. 1, 2022; accepted for publication Dec. 7, 2022; published online Jan. 10, 2023.

[DOI: 10.1117/1.AP.5.1.015001]

1 Introduction

Topological solitons with topologically protected spin texture are of fundamental interest in exploring fascinating physical phenomena and nonlinear field theories.[1] In particular, numerous low-dimensional topological solitonic textures have been extensively studied in recent years, such as one-dimensional magnetic domain walls and magnetic skyrmions,[2–4] as well as two-dimensional (2D) electromagnetic skyrmions,[5–8] merons, and bimerons.[9–11] Their sophisticated topological structures have been considered promising information carriers in the next generation of data storage and communication devices.[12–15] 3D topological textures have also been attracting considerable interest in condensed matter physics and optics, and, following their theoretical introduction, extending the frontiers of topological field manipulation.[13,16–18]

Hopfions, as the most classic 3D topological solitons, were initially proposed in the Skyrme–Faddeev model.[19–21] They are also known as Faddeev–Hopf knots[22,23] and can be elegantly mapped to a Hopf fibration and characterized by a Hopf index.[24,25] Hopfions have fundamental importance in many physical systems in high-energy physics,[26] chiral and frustrated magnets,[27–32] quantum fields,[33,34] condensed matter physics,[35–38] cosmology,[39,40] fluid dynamics,[41] liquid crystals,[42,43] and very recently, were realized in free-space photonics.[44] Due to their rich 3D spin texture, hopfions can potentially provide many opportunities in investigations and applications of topological structures. However, only a very limited number of hopfions have been experimentally realized to date. For instance, magnetic hopfions of Bloch (vortex) and Néel (hedgehog) types can be excited and exist in a stable state in chiral magnets.[28] In photonics, only fundamental-order hopfions with a unit Hopf index have been reported.[44] Spatial knot configurations of isophase in structured light fields have also been studied,[45–47] but they do not fulfill the 3D Hopf map. The generation and properties of higher-order photonic hopfions and their topological spin texture tuning have yet to be explored.

In this letter, we theoretically and experimentally demonstrate a generalized family of photonic hopfions constructed using superposition of paraxial Laguerre–Gaussian (LG) beams

*Address all correspondence to Yijie Shen, y.shen@soton.ac.uk; Zhihan Zhu, zhuzhihan@hrbust.edu.cn; Anatoly V. Zayats, a.zayats@kcl.ac.uk.

with customized polarization patterns. The generated complex vector fields have spatially varying 3D polarization distributions, which exhibit hopfion topological textures. The observed photonic hopfions can be freely transformed to various topological states, including Néel-type (hedgehog), Bloch-type (vortex), and antitype (saddle) textures and many intermediate topological classes. For each on-demand texture, a topological charge (Hopf index) of hopfions can also be tuned to arbitrary integers, realizing higher-order hopfions. We also demonstrate a free-space transport of hopfions with protected topology, revealing the potential to develop the technology of topological information transfer.

2 Results

In topology, a hopfion configuration is usually represented by a 3D real-space distribution of generalized unit spin vectors, $\mathbf{S}(x,y,z) = [s_x(x,y,z), s_y(x,y,z), s_z(x,y,z)]$, and achieved by a stereographic projection from a hypersphere $\mathbb{S}^3$ $[\boldsymbol{\chi} = (\chi_1,\chi_2,\chi_3,\chi_4)]$ to a real space $\mathbb{R}^3$ $[r = (x,y,z)]$, fulfilling the Hopf map $\mathbf{S} = \langle\boldsymbol{\zeta}|\boldsymbol{\sigma}|\boldsymbol{\zeta}\rangle$, where $|\boldsymbol{\zeta}\rangle = (\chi_4 + \mathrm{i}\chi_3, \chi_1 + \mathrm{i}\chi_2)^{\mathrm{T}}$ and $\boldsymbol{\sigma} = [\boldsymbol{\sigma}_x, \boldsymbol{\sigma}_y, \boldsymbol{\sigma}_z]$ correspond to the three Pauli matrices.[29] As a geometric representation of a Hopf map, a point on a $\mathbb{S}^2$ sphere (a so-called 2-sphere) corresponds to a closed line (loop) in a real space rather than a point in a real space, revealing the additional dimension of a hypersphere. Each loop corresponds to an isospin contour $[(s_x, s_y, s_z) = \text{const}]$ in the hopfion texture. Extending this description to optics, $\boldsymbol{\chi}$ components correspond to the real and imaginary parts of the complex-valued fields projected onto the circular polarization basis, thus capturing both polarization and phase variations in a 3D space. In turn, $\mathbf{S}$ is, therefore, formed by Stokes vectors (S_1, S_2, S_3), describing spatial variations of polarization of an optical field, and a 2-sphere is equivalent to a Poincaré sphere. In this framework, the isospin contours are isopolarization contours of an optical vector field.

An example of the mapping is illustrated in Fig. 1. Latitude, α, and longitude, β, of each point on a parametric 2-sphere, which represents a spin vector, are shown in Fig. 1(a) with hue color and lightness, respectively. The corresponding stereographic projection of an isopolarization contour in a real space is shown as a loop with the same color in Figs. 1(b) and 1(c). The loops mapped from the points on the same latitude β of a parametric sphere form a set of the torus knots (a set of knots that lies on the surface of a torus), completely covering a torus when scanning the points with different longitudes α [Fig. 1(b)]. Thus, the full unwrapping of the parametric sphere (for all latitudes and longitudes) results in the torus knots on the nested tori with each torus corresponding to different latitudes β, akin to matryoshka [Fig. 1(c)]; this construction is termed the Hopf fibration. In two extreme cases of the mapping, the spin-down contour (left circular polarization in optics), corresponding to the south pole of a 2-sphere, is the ring at the core of the nested tori (black line), whereas the spin-up contour (right circular polarization), corresponding to the north pole, is the line in the z direction along the axis of the nested tori.

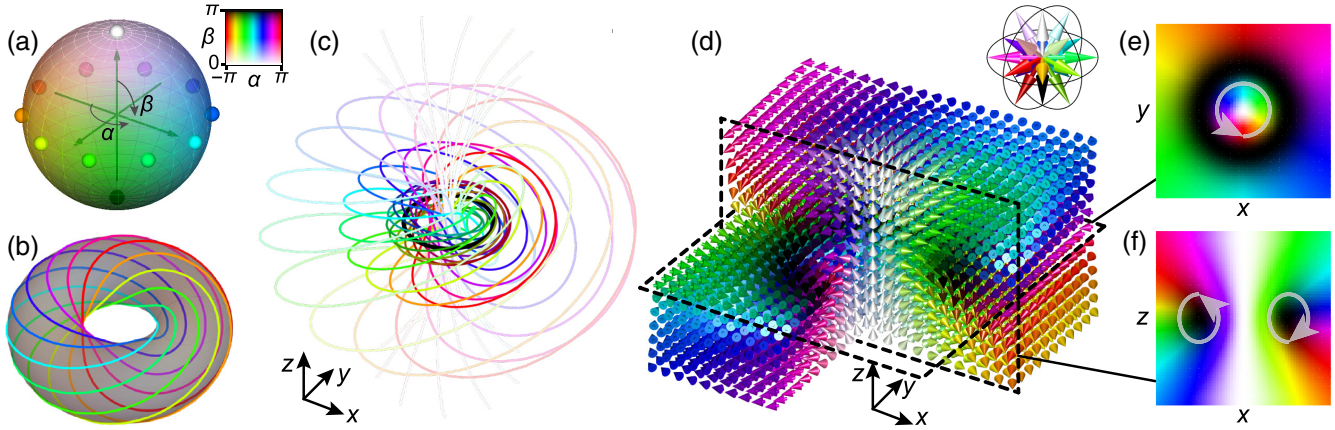

Fig. 1 (a) The parameter-space visualization of a hypersphere: the longitude and latitude degrees (α and β) of a parametric 2-sphere are represented by hue color and its lightness (dark towards the south pole, where spin is down, and bright towards the north pole, where spin is up). Each point on a parametric 2-sphere corresponds to a closed isospin line located in a 3D Euclidean space. (b) The lines projected from the selected points of the same latitude β and different longitude α on the hypersphere (highlighted by the solid dots with the corresponding hue colors) form torus knots covering a torus (with different tori corresponding to different β). (c) The real-space visualization of a Hopf fibration as a full stereographic mapping from a hypersphere: toroidally knotted lines (torus knots) arranged on a set of coaxially nested tori, with each torus corresponding to different latitude β of a parametric 2-sphere. The black circle corresponds to the south pole (spin down) and the axis of the nested tori corresponds to the north pole (spin up) in (a). (d) The 3D spin distribution in a hopfion, corresponding to the isospin contours in panel (c), with each spin vector colored by its α and β parameters of a parametric sphere in panel (a), as shown in the inset. (e), (f) The cross-sectional view of the spin distribution in panel (d): (e) x–y ($z = 0$) and (f) y–z ($x = 0$) cross sections show skyrmion-like structures with the gray arrows marking the vorticity of the skyrmions. Color scale corresponds to the spin direction in panel (d).

How knotted each torus knot is depends on the topological charge (Hopf index, Q_H) (see Supplementary Note I and Ref. 48). The Hopf index (topological charge) is determined by an around-torus index p and a through-torus index q via $Q_H = p \times q$, which describes how many times an isospin contour goes around the torus (p) and through the torus hole (q). A fundamental hopfion corresponds to one around and one through a torus configuration ($Q_H = 1$).

The 3D spin texture of a hopfion is shown in Fig. 1(d), where the colors of vectors correspond to the isospin contours in Fig. 1(c). A 3D hopfion is closely related to 2D skyrmions. Hopfion textures have a skyrmionium (a doughnut-shaped texture composed by two nested skyrmions with opposite polarities) in the x–y cross section at $z = 0$ [Fig. 1(e)], and the y–z cross section ($x = 0$) corresponds to two skyrmions with opposite vorticity and opposite skyrmion topological charges [Fig. 1(f)]. These are the signatures of a hopfion, since the hopfion can be represented by an end-to-end twisted skyrmion tube.[31] Due to the closed connection to skyrmions, hopfions can be classified by the type of skyrmionium in the x–y cross section, which in turn is classified by the type of 2D skyrmions forming it (see Supplementary Note II for details).[11–13]

The topological number of a hopfion (Hopf index) is defined by[25] $Q_H = p \times q = \frac{1}{(4\pi)^2}\iiint \mathbf{F}\cdot\mathbf{A}\mathrm{d}x\,\mathrm{d}y\,\mathrm{d}z$, where $F_i = \varepsilon_{ijk}\mathbf{S}\cdot(\partial_j\mathbf{S}\times\partial_k\mathbf{S})/2$, in which $i, j, k = \{x, y, z\}$, $\boldsymbol{\varepsilon}$ is the Levi–Civita tensor, and $\mathbf{A}$ is the vector potential satisfying $\nabla\times\mathbf{A} = \mathbf{F}$ and is closely related to the skyrmion number (p and q correspond to the skyrmion numbers of the skyrmions in the x–z and x–y cross sections of a hopfion[43]), which can be defined by the product of topological numbers of polarity Q_P and vorticity Q_V of the skyrmion spin texture.[13,49] The polarity $Q_P = \frac{1}{2}[\cos\beta(r)]_{r=0}^{r=a} = \pm 1$ is defined by the vector direction down (up) at the center $r = 0$ and up (down) at the skyrmion boundary $r \to r_\sigma$ for $Q_P = 1$ ($Q_P = -1$), and the vorticity $Q_V = \frac{1}{2\pi}[\alpha(\phi)]_{\phi=0}^{\phi=2\pi}$ can be an arbitrary integer that controls the azimuthal distribution of the transverse vector field components. For a fixed vorticity, an initial phase θ should be added to distinguish the helicity to completely decide the transverse distribution of the vector field, i.e., $\alpha(\phi) = m\phi + \theta$, which is termed helicity. For instance, a skyrmion with vorticity charge $Q_V = 1$ represents a hedgehog-like texture for a helicity $\theta = 0$ (named Néel Type-I), a squeezed hedgehog-like texture when helicity is π (named Néel Type-II), and a right- or left-handed vortex texture when helicity is $\pi/2$ or $3\pi/2$ (named Bloch type), whereas for the vorticity charge of -1, the skyrmion has a saddle-like texture (named antitype). The classification can be applied to hopfions, i.e., Néel, Bloch, antitype hopfions, given that the skyrmion appears in the x–y cross section of the hopfion.

Using structured light technologies to sculpture complex nonseparable states of an optical vector field,[50–52] a photonic hopfion can be constructed by the polarization Stokes vectors of a 3D-structured vector beam with the electric field given by $\boldsymbol{\psi}(x, y, z) = \psi_R(x, y, z)\hat{\mathbf{e}}_R + \psi_L(x, y, z)\hat{\mathbf{e}}_L$, where $\hat{\mathbf{e}}_R$ ($\hat{\mathbf{e}}_L$) is the eigenstate of right-handed (left-handed) circular polarization and ψ_R (ψ_L) is the corresponding spatial mode. The Stokes vector can be related to the electric field by $\mathbf{S} = \langle\boldsymbol{\psi}|\boldsymbol{\sigma}|\boldsymbol{\psi}\rangle$, using the same form of a Hopf map mentioned above. The developed experimental setup (see Supplementary Note III for the details of the experiment) allowed us to generate photonic hopfions with tunable topology via the interference of controlled LG beams and perform 3D tomography of the Stokes vectors distribution by measuring the spatial polarization distributions. The isopolarization contours exactly follow the Hopf fibration when $\psi_R = \mathrm{LG}_{0,0} + \mathrm{LG}_{1,0}$ and $\psi_L = \mathrm{LG}_{0,-1}$, where $\mathrm{LG}_{p,\ell}$ is the LG beam with radial index p and azimuthal (orbital angular momentum, OAM) index ℓ [Eq. (S17) in the Supplementary Material].[44] Arbitrary photonic hopfions can be obtained using interference of two LG beams, $\psi_R = \mathrm{LG}_{0,0} + e^{i\varphi}\mathrm{LG}_{1,0}$ and $\psi_L = e^{i\theta}\mathrm{LG}_{0,\ell}$, with two intermodal phases, φ and θ, that do not affect the configuration of the Hopf fibration.

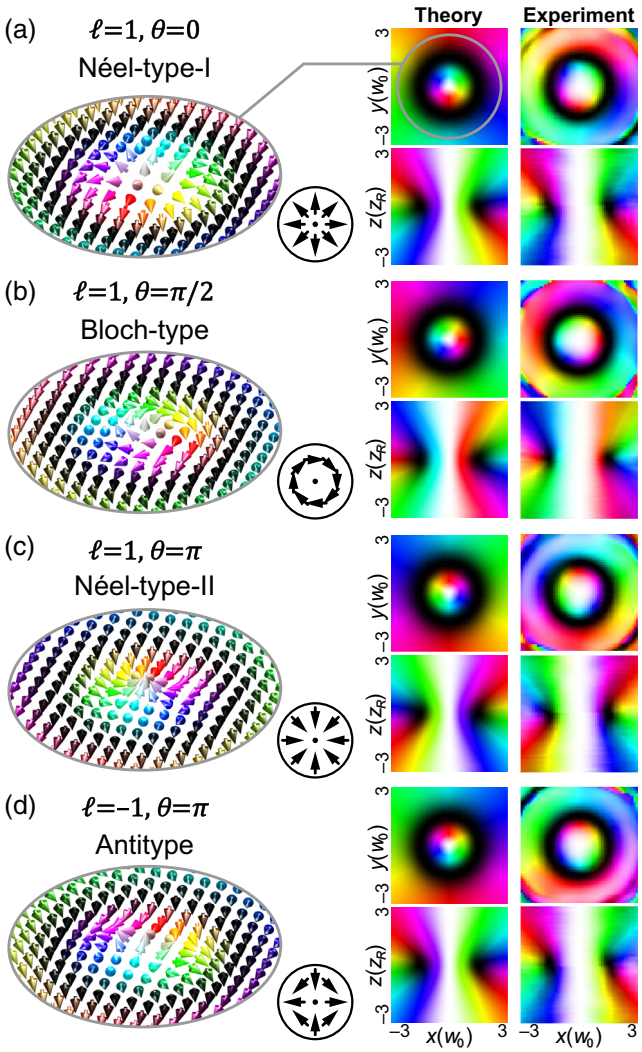

Fig. 2 Left, simulated Stokes vector distributions in the skyrmionium textures in the x–y ($z = 0$) plane of the photonic hopfions of (a) Néel Type-I ($Q_P = 1, Q_V = 1, \theta = 0$), (b) Bloch type ($Q_P = 1$, $Q_V = 1, \theta = \pi/2$), (c) Néel Type-II ($Q_P = 1, Q_V = 1, \theta = \pi$), and (d) antitype ($Q_P = 1, Q_V = -1, \theta = \pi$). The insets in black circles highlight the corresponding texture of the x–y components. Right, theoretical and experimental polarization distributions represented by Poincaré parameters (orientation and ellipticity of the polarization ellipse) in the x–y and y–z planes for the topological hopfions in panels (a)–(d). The x and y scales are normalized to the fundamental mode waist radius w_0, and the z-scale is normalized to the Rayleigh range z_R. The color scale is as shown in Fig. 1.

Topological protection of photonic hopfions is provided by the required Gouy phase difference [Eq. (S17) in the Supplementary Material] between the modal components. A finite size of a beam causes spread of the transverse wave vector components and a corresponding reduction of the longitudinal wave vector component, resulting in an additional (Gouy) phase. The three modal components must have a fixed ratio of the Gouy phases (e.g., $\mathrm{LG}_{0,0}/\mathrm{LG}_{0,-1}/\mathrm{LG}_{1,0} = 1:2:3$ for fundamental order hopfions), so that the hopfion topology can be stable and protected irrespectively of how absolute values of the intermodal phases change during propagation. In the opposite situation, for example, if the vortex component of the hopfion has mixed modes with the Gouy phases that do not satisfy the above condition, the beam will show a drastically variant structure upon propagation.[11,53]

Using the developed approach, photonic hopfions of arbitrary topological numbers Q_H and with all kinds of hopfionic textures can be generated, including Néel, Bloch, antitypes, and intermediate states. For example, choosing $\ell = 1$, the texture of a photonic hopfion can be switched by simply tuning θ between Néel Type-I ($\theta = 0$), Bloch type ($\theta = \pi/2$), Néel Type-II ($\theta = \pi$) [Figs. 2(a)–2(c)]. Choosing $\ell = -1$, the photonic hopfion of the antitype is observed in the case of $\theta = \pi$ [Fig. 2(d)]. The experimentally measured polarization distributions in the optical hopfions of Néel Type-I ($\ell = 1, \theta = 0$), Bloch type ($\ell = 1, \theta = \pi/2$), Néel Type-II ($\ell = 1, \theta = \pi$), and antitype ($\ell = -1, \theta = \pi$) are in excellent agreement with the theoretical results (Fig. 2).

In a fundamental-order hopfion, each fiber as a torus knot in the Hopf fibration goes one time through and one time around the torus, resulting in a topological charge of $Q_H = \pm 1$ ("±" decides chirality). For higher-order hopfions, if each torus-knot fiber goes p times through and q times around the torus, the topological charge is $Q_H = \pm p \times q$.[48] The vector fields of various higher-order hopfions can also be characterized by a closed-form expression related to p and q (see Supplementary Note I). Three examples of the torus-knot configurations of three higher-order hopfions with $(p, q) = (-2, 1)$, $(p, q) = (2, 1)$, and $(p, q) = (3, 2)$ were generated, using LG beams with $\ell > 1$ (Fig. 3). In general, for a given value of ℓ, the torus-knot indices are determined by $(p, q) = (\ell, |\ell| - 1)$. For each higher-order hopfion, the x–y cross section shows corresponding higher-order skyrmionium textures with vorticity equal to Q_H, and the y–z cross section shows two skyrmions with opposite higher-order vorticity.

In the past, a hopfion was always considered a static topological quasiparticle. Our developed approach provides a unique possibility to stimulate and observe free-space transport of hopfions with the preserved topology. This is achieved by tuning a phase parameter φ. In Figs. 2 and 3, $\varphi = 0$ and the hopfion center is located at $z = 0$. If the phase parameter is tuned, the hopfion configuration controllably propagates along the z axis (the hopfion center moves in a z direction). For example, when $\varphi = -\pi/2$, the hopfion is centered at $z = -z_R$ (where z_R is the Rayleigh length). When the value of φ is gradually increased to $\pi/2$, the hopfion center moves to $z = z_R$ (Fig. 4). The propagation can be explained and simulated considering the Gouy phase mediated intramodal phase changes. These lead to the variations of the amplitude profile of ψ_R along the radial direction upon propagation,[54] which determines the z-position of a 3D polarization texture of hopfions. As the initial intramodal phase φ is modified, the center of a hopfion ring, which corresponds to a plane with $\varphi = 0$, moves along the z direction (Supplementary Note IV).

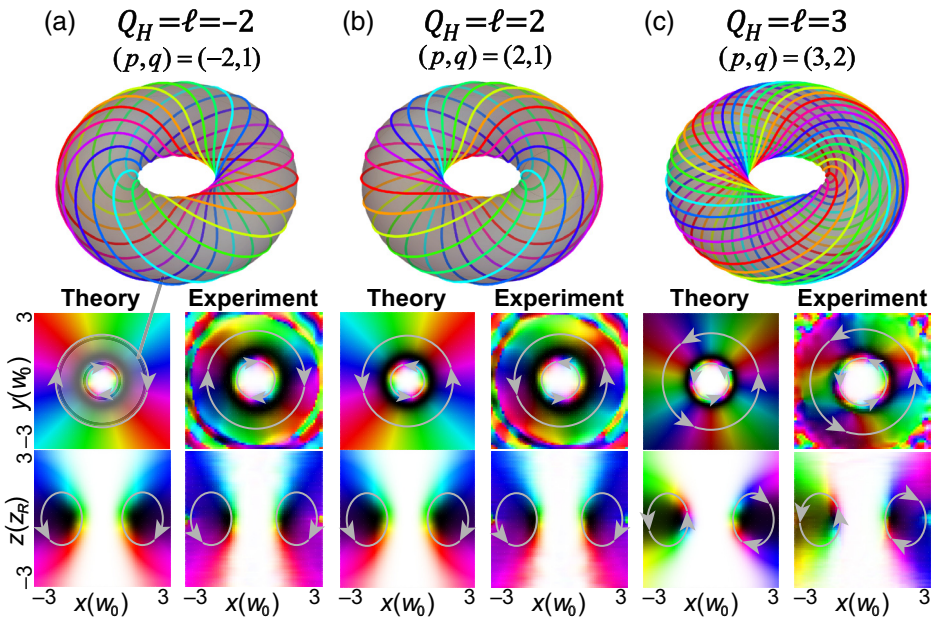

Fig. 3 (Top) The torus-knot configurations of a toroidal layer in the Hopf fibration for the higher-order hopfions with Hopf indices of (a) $Q_H = -2$, (b) $Q_H = 2$, and (c) $Q_H = 3$. (Bottom) Theoretical and experimental polarization distributions in the x–y and y–z planes for the hopfions in panels (a)–(c). Gray arrows indicate the vorticity. The geometric scales and the color scale are as shown in Fig. 2.

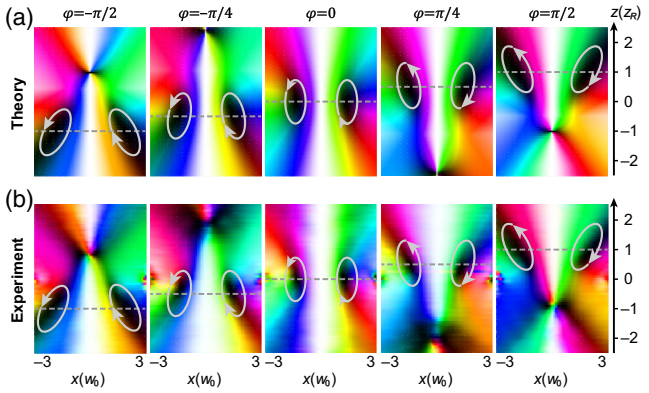

Fig. 4 Propagation of photonic hopfions in free space. (Top) Theoretical and (bottom) experimental polarization distributions in the x–z plane for different phases φ from $-\pi/2$ to $\pi/2$. The hopfion torus center moves along z from $z = -z_R$ to $z = z_R$ as φ changes. The gray dashed lines mark the location of hopfion torus centers. Gray arrows indicate the vorticity. The geometric scales and the color scale are as shown in Fig. 2.

3 Discussion and Conclusion

We presented both theoretical and experimental demonstrations of reconfigurable higher-order hopfionic textures and their free-space transport in paraxial structured light. The topological transformations between hopfions of Néel, Bloch, and antitypes were achieved, and the developed principle can be applied to other types of hopfions. The implemented mechanism to transport a hopfion structure maybe of interest for development of topological classical and quantum information carriers for optical communications and data manipulation, with robust topological protection against perturbations, such as scattering and disorder. Hopfions encompass the control of new topologies of structured light, which provides many degrees of freedom for these applications.

In this work, we studied optical hopfions in free space and realized their higher-order transformation with a controlled topological number. The described technique can be extended to other kinds of topological quasi-particles with sophisticated textures, such as torons[55] and heliknotons,[56] that were studied in solid-state systems but have never been explored in light fields. Because the topological numbers are mainly controlled by the OAM of a light field, the unresolved challenge is to achieve independent tuning of Hopf link numbers p and q.

It is also straightforward to generalize the results to an isotropic, nonmagnetic, and achiral medium, which would only introduce a scaling factor related to its refractive index. Similarly, media with the mode-independent gain and loss should also preserve the topological structure. A more complex and rich physics is expected for the optical hopfions in anisotropic, magnetic, and chiral media, or in the presence of strong mode-dependent gain and loss, which would influence the evolution of different modal components differently.

Acknowledgments

This work was supported, in part, by the National Natural Science Foundation of China (Grant Nos. 62075050, 11934013, and 61975047), the High-Level Talents Project of Heilongjiang Province (Grant No. 2020GSP12), and the European Research Council iCOMM project (Grant No. 789340). The authors declare no conflicts of interest.

Code, Data, and Materials Availability

Data underlying the results presented in this paper may be obtained from the authors upon reasonable request.

References

1. N. Manton and P. Sutcliffe, *Topological Solitons*, Cambridge University Press, Cambridge, UK (2004).
2. S. S. Parkin, M. Hayashi, and L. Thomas, "Magnetic domain-wall racetrack memory," *Science* **320**(5873), 190–194 (2008).
3. X. Wang et al., "Domain wall propagation through spin wave emission," *Phys. Rev. Lett.* **109**(16), 167209 (2012).
4. J. Han et al., "Mutual control of coherent spin waves and magnetic domain walls in a magnonic device," *Science* **366**(6469), 1121–1125 (2019).
5. S. Tsesses et al., "Optical skyrmion lattice in evanescent electromagnetic fields," *Science* **361**(6406), 993–996 (2018).
6. L. Du et al., "Deep-subwavelength features of photonic skyrmions in a confined electromagnetic field with orbital angular momentum," *Nat. Phys.* **15**(7), 650–654 (2019).
7. T. J. Davis et al., "Ultrafast vector imaging of plasmonic skyrmion dynamics with deep subwavelength resolution," *Science* **368**(6489), eaba6415 (2020).
8. Y. Shen et al., "Supertoroidal light pulses as electromagnetic skyrmions propagating in free space," *Nat. Commun.* **12**(1), 5891 (2021).
9. H. Jani et al., "Antiferromagnetic half-skyrmions and bimerons at room temperature," *Nature* **590**(7844), 74–79 (2021).
10. Y. Dai et al., "Plasmonic topological quasiparticle on the nanometre and femtosecond scales," *Nature* **588**(7839), 616–619 (2020).
11. Y. Shen, "Topological bimeronic beams," *Opt. Lett.* **46**(15), 3737–3740 (2021).
12. Y. Shen, E. C. Martínez, and C. Rosales-Guzmán, "Generation of optical skyrmions with tunable topological textures," *ACS Photonics* **9**(1), 296–303 (2022).
13. B. Göbel, I. Mertig, and O. A. Tretiakov, "Beyond skyrmions: review and perspectives of alternative magnetic quasiparticles," *Phys. Rep.* **895**, 1–28 (2021).
14. A. Fert, N. Reyren, and V. Cros, "Magnetic skyrmions: advances in physics and potential applications," *Nat. Rev. Mater.* **2**(7), 17031 (2017).
15. B. A. Bernevig, C. Felser, and H. Beidenkopf, "Progress and prospects in magnetic topological materials," *Nature* **603**(7899), 41–51 (2022).
16. P. J. Ackerman and I. I. Smalyukh, "Static three-dimensional topological solitons in fluid chiral ferromagnets and colloids," *Nat. Mater.* **16**(4), 426–432 (2017).
17. J. Tang et al., "Magnetic skyrmion bundles and their current-driven dynamics," *Nat. Nanotechnol.* **16**, 1086–1091 (2021).
18. F. Zheng et al., "Magnetic skyrmion braids," *Nat. Commun.* **12**, 5316 (2021).
19. L. Faddeev, "Some comments on the many-dimensional solitons," *Lett. Math. Phys.* **1**(4), 289–293 (1976).
20. T. H. R. Skyrme, "A non-linear field theory," *Proc. R. Soc. A* **260**, 127–138 (1961).
21. T. H. R. Skyrme, "A unified field theory of mesons and baryons," *Nucl. Phys.* **31**, 556–569 (1962).
22. J. Hietarinta and P. Salo, "Faddeev-Hopf knots: dynamics of linked un-knots," *Phys. Lett. B* **451**(1-2), 60–67 (1999).
23. P. Sutcliffe, "Knots in the Skyrme–Faddeev model," *Proc. R. Soc. A: Math. Phys. Eng. Sci.* **463**(2087), 3001–3020 (2007).
24. D. W. Lyons, "An elementary introduction to the Hopf fibration," *Math. Mag.* **76**(2), 87–98 (2003).

25. J. Whitehead, "An expression of Hopf's invariant as an integral," *Proc. Natl. Acad. Sci. U.S.A.* **33**(5), 117–123 (1947).
26. L. Faddeev and A. J. Niemi, "Stable knot-like structures in classical field theory," *Nature* **387**(6628), 58–61 (1997).
27. J.-S. B. Tai et al., "Static Hopf solitons and knotted emergent fields in solid-state noncentrosymmetric magnetic nanostructures," *Phys. Rev. Lett.* **121**(18), 187201 (2018).
28. X. Wang, A. Qaiumzadeh, and A. Brataas, "Current-driven dynamics of magnetic hopfions," *Phys. Rev. Lett.* **123**(14), 147203 (2019).
29. Y. Liu et al., "Three-dimensional dynamics of a magnetic hopfion driven by spin transfer torque," *Phys. Rev. Lett.* **124**(12), 127204 (2020).
30. I. Luk'yanchuk et al., "Hopfions emerge in ferroelectrics," *Nat. Commun.* **11**(1), 2433 (2020).
31. B. Göbel et al., "Topological hall signatures of magnetic hopfions," *Phys. Rev. Res.* **2**(1), 013315 (2020).
32. N. Kent et al., "Creation and observation of hopfions in magnetic multilayer systems," *Nat. Commun.* **12**(1), 1562 (2021).
33. D. S. Hall et al., "Tying quantum knots," *Nat. Phys.* **12**(5), 478–483 (2016).
34. W. Lee et al., "Synthetic electromagnetic knot in a three-dimensional skyrmion," *Sci. Adv.* **4**(3), eaao3820 (2018).
35. E. Babaev, "Dual neutral variables and knot solitons in triplet superconductors," *Phys. Rev. Lett.* **88**(17), 177002 (2002).
36. Y. Kawaguchi, M. Nitta, and M. Ueda, "Knots in a spinor Bose-Einstein condensate," *Phys. Rev. Lett.* **100**(18), 180403 (2008).
37. R. Bisset et al., "Robust vortex lines, vortex rings, and hopfions in three-dimensional Bose-Einstein condensates," *Phys. Rev. A* **92**(6), 063611 (2015).
38. S. Zou et al., "Formation of vortex rings and hopfions in trapped Bose–Einstein condensates," *Phys. Fluids* **33**(2), 027105 (2021).
39. M. Cruz et al., "A cosmic microwave background feature consistent with a cosmic texture," *Science* **318**(5856), 1612–1614 (2007).
40. A. Thompson et al., "Classification of electromagnetic and gravitational hopfions by algebraic type," *J. Phys. A: Math. Theor.* **48**(20), 205202 (2015).
41. D. Kleckner and W. T. Irvine, "Creation and dynamics of knotted vortices," *Nat. Phys.* **9**(4), 253–258 (2013).
42. P. J. Ackerman and I. I. Smalyukh, "Diversity of knot solitons in liquid crystals manifested by linking of preimages in torons and hopfions," *Phys. Rev. X* **7**(1), 011006 (2017).
43. P. J. Ackerman, J. Van De Lagemaat, and I. I. Smalyukh, "Self-assembly and electrostriction of arrays and chains of hopfion particles in chiral liquid crystals," *Nat. Commun.* **6**(1), 6012 (2015).
44. D. Sugic et al., "Particle-like topologies in light," *Nat. Commun.* **12**(1), 6785 (2021).
45. M. R. Dennis et al., "Isolated optical vortex knots," *Nat. Phys.* **6**(2), 118–121 (2010).
46. Y. Intaravanne et al., "Color-selective three-dimensional polarization structures," *Light Sci. Appl.* **11**(1), 302 (2022).
47. C. Wan et al., "Scalar optical hopfions," *eLight* **2**(1), 22 (2022).
48. M. Kobayashi and M. Nitta, "Torus knots as hopfions," *Phys. Lett. B* **728**, 314–318 (2014).
49. Y. Shen et al., "Topological quasiparticles of light: optical skyrmions and beyond," arXiv:2205.10329 (2022).
50. Y. Shen, "Rays, waves, SU(2) symmetry and geometry: toolkits for structured light," *J. Opt.* **23**(12), 124004 (2021).
51. Y. Shen and C. Rosales-Guzmán, "Nonseparable states of light: from quantum to classical," *Laser Photonics Rev.* **16**, 2100533 (2022).
52. C. He, Y. Shen, and A. Forbes, "Towards higher-dimensional structured light," *Light Sci. Appl.* **11**(1), 205 (2022).
53. S. Gao et al., "Paraxial skyrmionic beams," *Phys. Rev. A* **102**(5), 053513 (2020).
54. R.-Y. Zhong et al., "Gouy-phase-mediated propagation variations and revivals of transverse structure in vectorially structured light," *Phys. Rev. A* **103**(5), 053520 (2021).
55. G. Poy et al., "Interaction and co-assembly of optical and topological solitons," *Nat. Photonics* **16**, 454–461 (2022).
56. J.-S. B. Tai and I. I. Smalyukh, "Three-dimensional crystals of adaptive knots," *Science* **365**(6460), 1449–1453 (2019).

Yijie Shen received his PhD in optical engineering from Tsinghua University, Beijing, China, in 2019. Currently, he is a senior research fellow at Optoelectronics Research Centre (ORC), University of Southampton, United Kingdom. He was also a visiting researcher at the Structured Light Laboratory, School of Physics, University of the Witwatersrand (Wits University), Johannesburg, South Africa, in 2019. His research interests include structured light, ultrafast nonlinear optics, quantum optics, metamaterial, and nanophotonics.

Bingshi Yu received his BSc degree in applied physics from Harbin University of Science and Technology, China, in 2021. Currently, he is pursuing an MS degree at the Quantum Optics Laboratory led by Zhihan Zhu and Carmelo Rosales-Guzmán at the Harbin University of Science and Technology. His research interests include shaping and characterizing photons' full spatiotemporal amplitude, phase, and spin structures.

Haijun Wu received his BSc degree in applied physics from Harbin University of Science and Technology, China, in 2018. He joined the Quantum Optics Laboratory led by Zhihan Zhu and Carmelo Rosales-Guzmán and received his MS degree in physics in 2020. Currently, he is pursuing a PhD at the same laboratory. His research interests include shaping and controlling structured photons via nonlinear interactions.

Chunyu Li received her BSc degree in applied physics from Harbin University of Science and Technology, China, in 2020. Currently, she is pursuing a PhD at the Quantum Optics Laboratory led by Zhihan Zhu and Carmelo Rosales-Guzmán at the Harbin University of Science and Technology. Her research interests include shaping and controlling light full spatiotemporal structure via geometric-phase elements.

Zhihan Zhu received his PhD in optics from Harbin University of Science and Technology in 2017, where he established Quantum Optics Group and Laboratory. Currently, he is a professor of optics at Heilongjiang Key Laboratory of Quantum Control in Harbin (China). His research interests include quantum and nonlinear optics with structured light, especially for generation and manipulation of structured photons via nonlinear interactions.

Anatoly V. Zayats is Chair in experimental physics and head of the Photonics & Nanotechnology at the Department of Physics, King's College London. He is a co-director of the London Centre for Nanotechnology and the London Institute for Advanced Light Technologies. His research interests include nanophotonics and plasmonics, metamaterials and metasurfaces, electromagnetic field topology and optical spin-orbit coupling, and nonlinear and ultrafast optics.